was kept at 37°C overnight to introduce ^{125}I residue into the amino groups of pSV-LacZ. Noncoupled, free ^{125}I-labeled reagent was removed from ^{125}I-labeled pSV-LacZ solution by gel filtration with a PD10 column (Amersham Pharmacia Biotech, Tokyo, Japan).

Preparation of cationized gelatin microspheres incorporating pCMV-MMP

Gelatin microspheres were prepared through glutaraldehyde cross-linking of cationized gelatin aqueous solution according to a method reported previously, with slight modification.[16] Briefly, 5 ml of 10wt% gelatin aqueous solution preheated at 40°C for 1 h was added dropwise into 175 mL of olive oil under stirring at 420 rpm for 10 min at 40°C to prepare a water-in-oil emulsion. The emulsion was cooled to 4°C and agitated for 1 h. After addition of 50 mL of acetone, the emulsion was further stirred at 300 rpm for 1 h. The resulting microspheres were washed three times with acetone and put through sieves with apertures of 50 and 90 μm, and collected in the in-between size.

Non-cross-linked and air-dried gelatin microspheres (5 mg) were placed in a mixed solution of 14 mL of acetone and 6 mL of 0.01 M HCl aqueous solution containing glutaraldehyde (60 μg/mL) and stirred at 4°C for 24 h to facilitate cross-linking. After collection by centrifugation (5000 rpm, 4°C, 5 min), the microspheres were agitated in 100 mL of 100 mM aqueous glycine solution at 25°C for 1 h to block the residual aldehyde groups on unreacted glutaraldehyde. The resulting microspheres were washed three times with doubly distilled water by centrifugation and freeze-dried. The water content of the microspheres prepared was calculated from their volume before and after swelling in saline for 24 h at room temperature. Both wet and freeze-dried microspheres (at least 100 each) were viewed with a light microscope to measure their diameter, from which the volume of the respective microspheres was calculated. When calculated by the volume ratio of water to the wet microspheres, the water content of gelatin microspheres used was 94.7vol%. The average diameter of microspheres after swelling in saline was 73 μm.

Cationized gelatin microspheres incorporating pCMV-MMP were obtained by dropping 10 μL of aqueous solution containing 50 μg of pCMV-MMP onto 1 mg of freeze-dried gelatin microspheres, left at 25°C for 30 min to allow the pCMV-MMP solution to impregnate the dried microspheres. The solution was completely absorbed by the microspheres during the impregnation process, because the solution volume was much less than that theoretically required to fully impregnate into the microspheres. Empty gelatin microspheres without pCMV-MMP were prepared similarly except for the use of pCMV-MMP-free phosphate-buffered saline solution (PBS, pH 7.4).

Animal experiments

All the procedures were performed in accordance with specifications of the *Guidelines for Animal Experiments* of Kyoto University. C57BL/6 female mice (6 weeks old; body weight, ~15 g; Shimizu Laboratory Supplies, Kyoto, Japan) were housed in a specific pathogen-free facility and were maintained on standard mouse chow and tap water *ad libitum*. Each invasive treatment was performed under sufficient anesthesia by pentobarbital intraperitoneally administered (15 mg/kg body weight).

Preparation of cationized gelatin hydrogels incorporating pSV-LacZ

Impregnation of pSV-LacZ into freeze-dried cationized gelatin hydrogels was carried out by use of PBS containing 100 μg of pSV-LacZ. pSV-LacZ-free, empty cationized gelatin hydrogels were prepared in a similar way except for the use of pSV-LacZ-free PBS. Briefly, 20 μL of PBS with or without pSV-LacZ was dropped onto dried hydrogel granules, followed by leaving them at 4°C overnight to obtain cationized gelatin hydrogels incorporating pSV-LacZ or hydrogels without pSV-LacZ incorporation. Similarly, an aqueous solution of ^{125}I-labeled pSV-LacZ was sorbed into freeze-dried cationized gelatin hydrogel granules to prepare cationized gelatin hydrogels incorporating ^{125}I-labeled pSV-LacZ.

Estimation of in vivo *degradation of cationized gelatin hydrogels*

^{125}I-labeled cationized gelatin hydrogel granules were implanted into the femoral muscle of mice. At 1, 3, 7, 10, 14, and 21 days after hydrogel implantation, mouse muscle containing the implanted hydrogel granules was taken out to measure their radioactivity with a γ counter (ARC-301B; Aloka, Tokyo, Japan). The radioactivity ratio of the muscle sample to the hydrogel granules implanted initially was measured to express the percentage of remaining activity in the hydrogel granules.

Estimation of in vivo *pSV-LacZ release from cationized gelatin hydrogels incorporating pSV-LacZ*

After implantation of ^{125}I-labeled pSV-LacZ-incorporated cationized gelatin hydrogel granules into the femoral muscle of mice at different time intervals, the mouse muscles containing cationized gelatin hydrogel granules were taken out. As a control, the solution of ^{125}I-labeled pSV-LacZ in PBS was injected into the femoral muscle (100 μL/site). The radioactivity of the muscle samples was measured with a γ counter and the ratio to the initial radioactivity of hydrogels or pSV-LacZ solution injected was measured to express the percentage of radioactivity remaining. For each experimental group,

three mice were killed at each time point for *in vivo* evaluation.

In vivo *assessment of gene expression after implantation of cationized gelatin hydrogel granules incorporating pSV-LacZ*

pSV-LacZ-incorporated cationized gelatin hydrogels were implanted into the femoral muscle of mice. As a control, 100 μL of pSV-LacZ solution was intramuscularly injected into each mouse. The pSV-LacZ dose was 100 μg/mouse and three mice were used at each time point for every experimental group. The mice were killed 1, 3, 7, 14, 21, and 28 days after pSV-LacZ treatment to evaluate gene expression.

For evaluation of gene expression at the treated muscle, β-galactosidase activity was measured by use of a kit (Invitrogen, Carlsbad, CA). Briefly, muscle samples were immersed and homogenized in lysis buffer (0.1 M Tris-HCl, 2 mM EDTA, 0.1% Triton X-100) at a lysis buffer volume (mL)-to-sample weight (mg) ratio of 4 to 1 in order to normalize the influence of weight variance on the β-galactosidase assay. Sample lysate (2 mL) was transferred to a centrifuge tube, followed by freeze–thawing three times and centrifugation at 14,000 rpm at 4°C for 5 min. The supernatant (30 μL) was mixed with 70 μL of aqueous solution containing *o*-nitrophenyl-β-D-galactopyranoside (ONPG), 4 mg/mL) and 200 μL of cleavage buffer (60 mM $Na_2HPO_4 \cdot 7H_2O$, 40 mM $NaH_2PO_4 \cdot H_2O$, 10 mM KCl, and 1 mM $MgSO_4 \cdot 7H_2O$, pH 7) in a fresh microcentrifuge tube. After incubation at 37°C for 30 min, 500 μL of 1 M sodium carbonate solution was added to the solution mixture. The solution absorbance was measured at a wavelength of 420 nm to evaluate the β-galactosidase activity.

Prophylactic experiment involving tissue sclerosis in mouse kidney

Under sufficient anesthesia, a left flank incision was made from the edge of the left rib to the paraumbilical area of mice, leading to exposure of the left kidney. Microspheres with or without 50 μg of pCMV-MMP were dispersed in 100 μL of saline. Left renal vessels were clamped and the microspheres were injected into the subcapsule of the left kidney with a 27-gauge needle, and the clamp was removed 10 min after injection. As controls, 100 μL of PBS or 100 μl of PBS containing 50 μg of pCMV-MMP was injected in the same way. The wound was closed with bilayer suturing.

Mice were injected via the tail vein with a bolus injection of streptozotocin (STZ, 200 mg/kg) dissolved in citrate buffer (pH 4.8) 7 days after operation, under light ether anesthesia. Induction of diabetes in mice was confirmed by measuring the plasma concentration of glucose by the conventional glucose oxidase method[17] 21 days after STZ injection (analyzed by autoanalyzer; Falco Biosystems, Kyoto, Japan). Mice were killed by cervical dislocation, followed by the harvesting of blood and left kidney 28 days after STZ injection. Plasma creatinine and serum blood urea nitrogen (BUN) levels were measured by conventional autoanalyzer (Falco Biosystems). Each experimental group comprised five mice. One part of the kidney was fixed in 10% phosphate-buffered formalin and paraffin embedded. Cross-sections (4 μm thick) were prepared and stained with Masson's trichrome to histologically view the fibrotic extent of tissue (AX-80; Olympus, Tokyo, Japan). The other part was immediately snap-frozen in liquid nitrogen and stored at −80°C for hydroxyproline determination.

Hydroxyproline determination

Hydroxyproline was determined according to the Kivirikko–Laitinen–Prockop method.[18] Briefly, kidney specimens were dried and hydrolyzed in 6 N HCl at 110°C for 24 h. The acidic solution was neutralized with 8 N KOH with phenolphthalein as a pH indicator, and solid KCl was added to 2 mL of the neutralized solution until saturation. The solution was mixed with 125 μL of β-alanine solution (pH 8.7) and 250 μL of borate-buffered solution (pH 8.2) for 30 min at 25°C and 250 μL of chloramine-T solution (1.41 g of chloramine-T per 25 mL of 2-methoxyethanol) was added to the mixed solution and left at 25°C for 25 min. After adding 750 μL of 3.6 M sodium thiosulfate solution, 1.25 mL of toluene was overlaid on the solution and mixed intensely for 5 min. The toluene layer was carefully removed after centrifugation (1500 rpm, 5 min), and the remaining solution was incubated at 100°C for 30 min. After cooling by flowing water, 1.25 mL of toluene was added to the solution and vigorous mixing was performed for 5 min again. After centrifugation and careful removal of the toluene layer, 250 μL of *p*-dimethylbenzaldehyde solution (mixture solution of 15 g of *p*-dimethylbenzaldehyde in 25 mL of ethanol and 6.25 g of conc. H_2SO_4 in 25 mL of ethanol) was added and placed at 25°C for 30 min. The absorbance of the resulting solution was measured spectrophotometrically at a wavelength of 560 nm. The calibration reference was measured with hydroxypoline solution at given concentrations. Data obtained were normalized by the dry weight of each tissue sample (mg/g dry tissue).

Immunofluorescence microscopic observation

In vivo expression of MMP-1 protein was confirmed as coexpression by immunofluorescence examination, using a rabbit anti-MMP-1 antibody and a mouse anti-FLAG antibody, in mouse kidney. Microspheres incorporating 50 μg of pCMV-MMP-FLAG were injected for immunofluorescence study. Kidney samples were taken

2 days after operation and embedded in Tissue-Tek (O.C.T. compound; Sakura Finetek U.S.A., Torrance, CA). Another immunofluorescence study was performed to investigate MMP-1 expression and its distribution 7 days after administration of microspheres incorporating 50 μg of pCMV-MMP. Cryosections (5 μm thick) were prepared from the embedded sample and fixed with 4% paraformaldehyde for 30 min. After washing them with PBS twice at 25°C, immunofluorescence examination was performed by using an M.O.M. immunodetection kit (Vector Laboratories, Burlingame, CA). Each fixed section was incubated with M.O.M. mouse IgG blocking reagent (lot M0314) for 1 h.

Anti-MMP-1 antibody solution (rabbit anti-MMP-1 monoclonal antibody, 1 μg/mL) was diluted 100 times with M.O.M. diluent (lot M0914) and sections were incubated with the diluted antibody solution at 25°C for 1 h. After rinsing with washing buffer (10 × PBS, 100 mL; 0.5% saponin, 10 mL; DDW, 890 mL) for 20 min (three at 25°C), the sections were incubated with diluted mouse anti-FLAG antibody solution containing antibody at 1 μg/mL, followed by additional rinses with washing buffer for 20 min (three times at 25°C). The sections were then incubated with the diluted mixture of anti-rabbit IgG–RITC conjugate and anti-mouse IgG–FITC conjugate for 1 h at 25°C. Finally, the stained sections were rinsed with washing buffer for 2 min (four times at 25°C) and PBS briefly, mounted with VectaShield mounting medium (Vector Laboratories), and examined for localization of MMP protein and FLAG antigen, using an Olympus AX-80 fluorescence microscope equipped with an Olympus DP50 digital camera. Cryosections derived from mice 7 days after receiving microspheres incorporating 50 μg of pCMV-MMP were analyzed in the same way, using anti-MMP-1 antibody solution and anti-rabbit IgG–RITC.

Statistical analysis

All data were expressed as means ± the standard error of the mean and statistically analyzed by Student t test, to be accepted as significant at $p < 0.05$.

RESULTS

Figure 1 shows the decrement patterns of pSV-LacZ and radioactivity after implantation of cationized gelatin hydrogels incorporating ^{125}I-labeled pSV-LacZ and, simultaneously, the time course of radioactivity remaining after implantation of ^{125}I-labeled cationized gelatin hydrogels into the femoral muscle of mice. The residual radioactivity of pSV-LacZ in cationized gelatin hydrogels decreased with implantation time period and the decrement pattern of radioactivity of pSV-LacZ and cationized gelatin hydrogels was significantly accommodative. On the other hand, for free ^{125}I-labeled pSV-LacZ radioactivity rapidly disappeared from the injected site within 3 days.

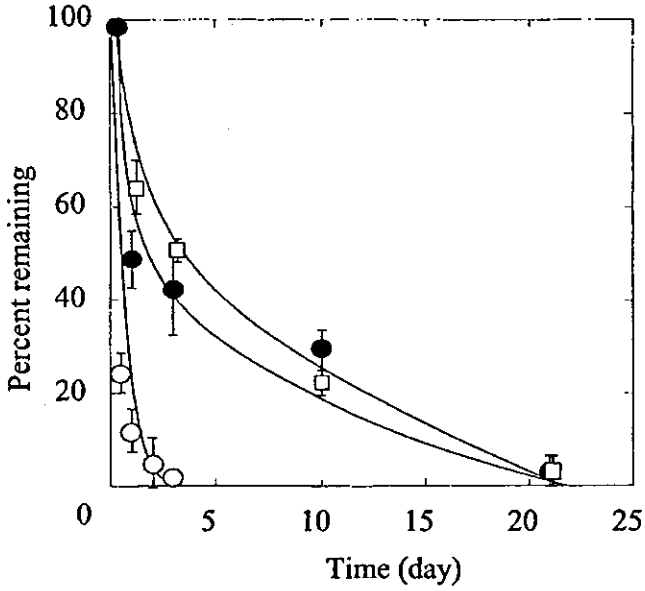

FIG. 1. The time course of radioactivity remaining in cationized hydrogel granules incorporating ^{125}I-labeled pSV-LacZ (●) and ^{125}I-labeled cationized hydrogel granules (□) after implantation into the femoral muscle of mice. (○) Radioactivity remaining after the intramuscular injection of ^{125}I-labeled pSV-LacZ in solution form. Three cationized gelatin hydrogels were used for every experiment.

Figure 2 shows the time course of gene expression after intramuscular implantation of cationized gelatin hydrogel granules incorporating pSV-LacZ or injection of PBS containing pSV-LacZ. The injection of pSV-LacZ solution showed significant gene expression only 3 days after injection; thereafter expression returned to the basal level. On the other hand, cationized gelatin hydrogel granules incorporating pSV-LacZ significantly enhanced the expression level as well as prolonged the duration time period. The level of gene expression increased within 3 days of implantation of the hydrogel granules and was maintained longer than that of pSV-LacZ solution.

Figure 3 shows an immunofluorescent microscopic section of mouse kidney administered microspheres incorporating pCMV-MMP-FLAG. The localization of MMP-1 protein together with FLAG antigen was observed around the site of administration of the microspheres. The MMP-1 protein secreted *de novo* was detected in the cortical part of the mouse kidney, and the microspheres remained in the subcapsule for 2 days after administration. The mouse kidney that received microspheres incorporating pCMV-MMP showed sustained expression even on day 7 in the renal tissue.

Table 1 shows the serum biochemical parameters of STZ-induced diabetic mice preadministered pCMV-

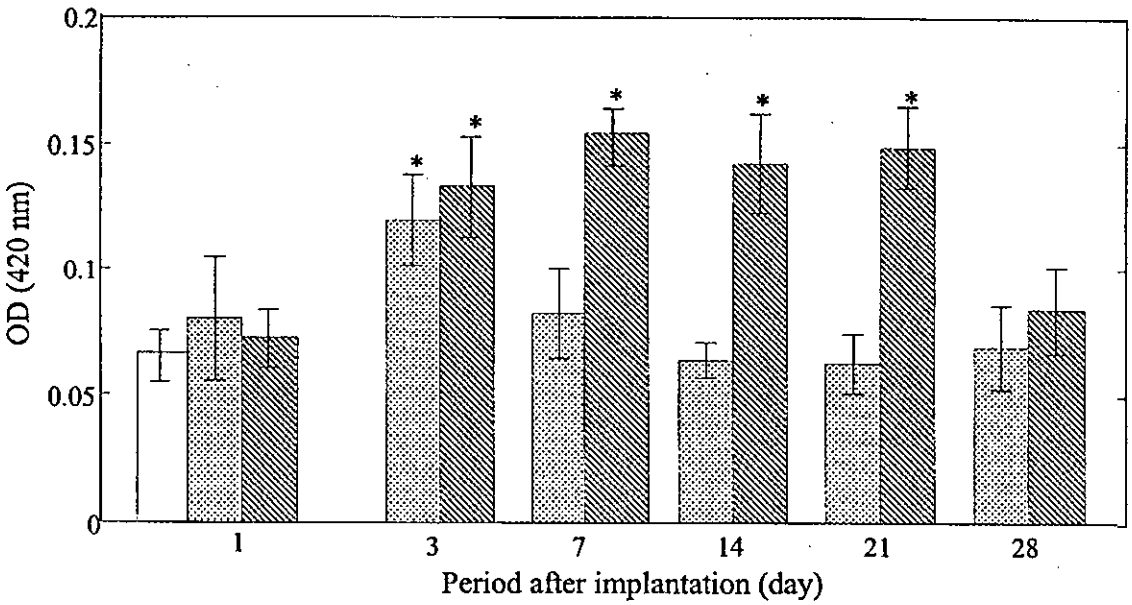

FIG. 2. The time course of *lacZ* gene expression after implantation of cationized gelatin hydrogel granules incorporating pSV-LacZ into the femoral muscle of mice: open columns, PBS; dotted columns, pSV-LacZ solutions; hatched columns, cationized gelatin hydrogel granules incorporating pSV-LacZ. The pSV-LacZ dose is 100 μg/mouse muscle. *$p < 0.05$: significant against the OD value of untreated, normal mice.

MMP or other agents. Blood glucose levels exceeded 300 mg of glucose/dL 3 weeks after STZ injection in all groups. Preadministration of microspheres incorporating pCMV-MMP significantly decreased the BUN level in the STZ-induced diabetic nephropathy model, in marked contrast to other groups, whereas the blood level of serum creatinine did not recover with the injection of microspheres incorporating pCMV-MMP. The administration of free pCMV-MMP solution may decrease the BUN level in this model, although no significant effect was achieved.

Figure 4 shows the amount of hydroxyproline in the kidney of STZ-induced diabetic mice preadministered pCMV-MMP or other agents. Hydroxyproline was decreased by preadministration of cationized gelatin microspheres incorporating pCMV-MMP and free pCMV-MMP to a significantly greater extent compared with administration of PBS and pCMV-MMP-free gelatin microspheres. This result indicates that excess type I collagen, a prime contributor to tissue fibrosis, was effectively digested by induction of the MMP-1 gene in mouse kidney.

Figure 5 shows histological renal sections of mice preadministered microspheres incorporating pCMV-MMP or other agents 28 days after STZ injection. Renal fibrosis was histologically suppressed by the application of cationized gelatin microspheres incorporating pCMV-MMP, compared with that of free pCMV-MMP. The administration of pCMV-MMP-free gelatin microspheres was not effective; the tissue appeared similar to that of the PBS-administered control group.

DISCUSSION

Destructive fibrosis is one of the features most commonly observed in progressive renal diseases. The fibrotic change is generally characterized by qualitative alteration of ECM components, such as collagen of type I and III, which is caused by the impaired turnover of ECM. The present study was undertaken to examine whether a fibrolytic enzyme, MMP, is effective in preventing the progress of diabetic renal sclerosis, as MMP may attenuate the increasing fibrous tissue in the fibrogenic phase of renal sclerosis, leading to the restoration of impaired matrix turnover.[10]

MMPs compose a family of zinc-dependent enzymes that degrade all the proteineous components of connective tissues. Currently, 26 human MMPs have been identified and are classified on the basis of substrate specificity and structural similarity. There are four major subgroups: (1) interstitial collagenase, (2) gelatinase, (3) stromelysin, and (4) MT-MMP.[19] MMP-1 is an interstitial collagenase and plays an important role at an initial step and throughout the fibrolysis process, which involves multiple steps; that is, it degrades the structural collagens of types I, II, and III, with the characteristic cleavage site for type I collagen at G-775/L-776.[20,21] Therefore, it is less possible for fibrolytic treatment with MMP-1 to generate unexpected effects than treatment with growth factors.

Theoretically speaking, MMP-1 may have only limited potential to repair damaged tissue. From the viewpoint of tissue engineering, the main components required are cells,

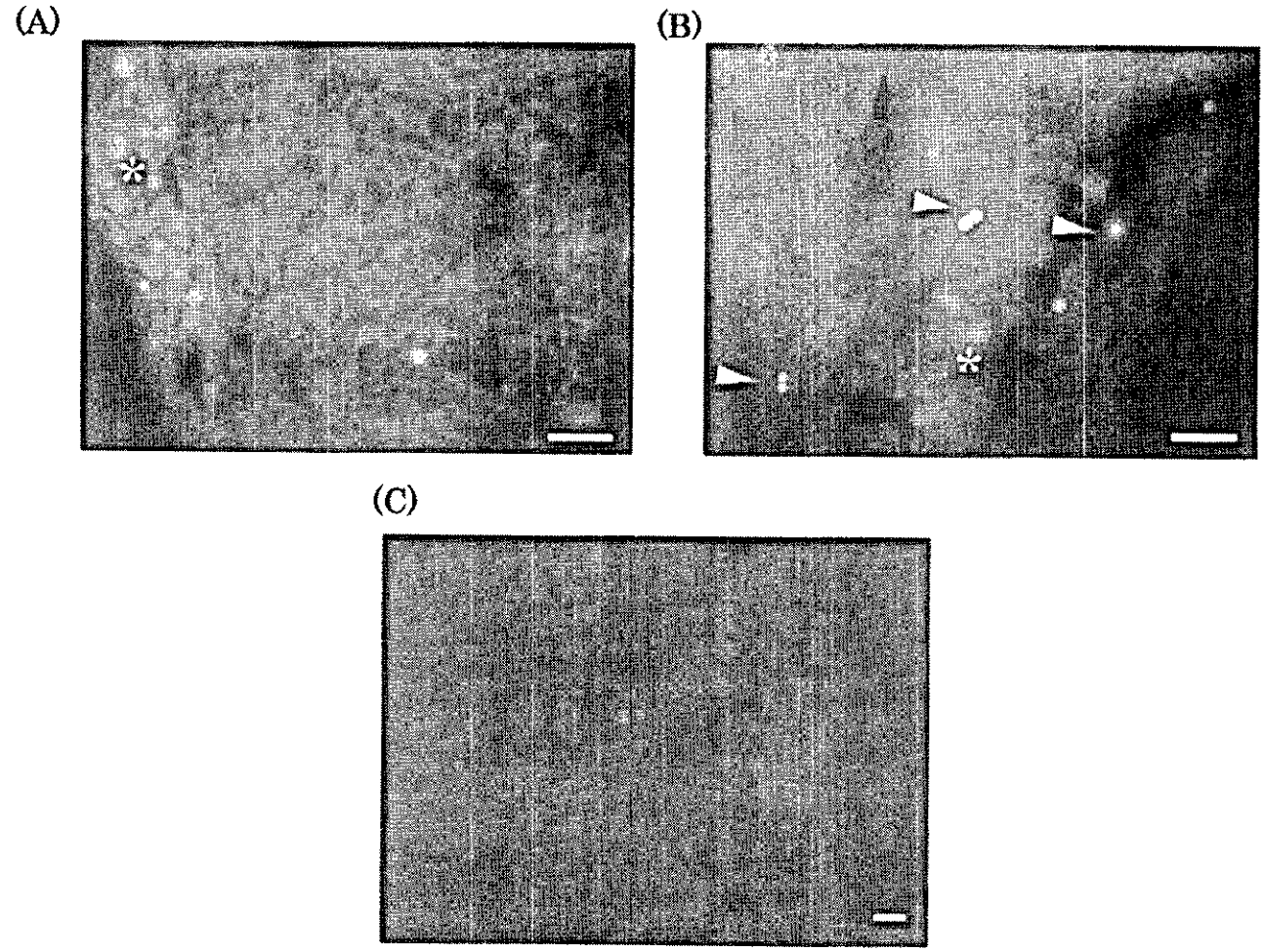

FIG. 3. Immunofluorescent microscopic sections of mouse kidneys 2 days (**A** and **B**) and 7 days (**C**) after administration of gelatin microspheres incorporating pCMV-MMP-FLAG (**A** and **B**) and pCMV-MMP (**C**) into the renal subcapsule (50 μg of pCMV-MMP-FLAG or pCMV-MMP per site). (**A**) Immunofluorescent image without first antibody; (**B**) immunofluorescent image of MMP-1 protein (visualized with RITC) and FLAG antigen (visualized with FITC); (**C**) immunofluorescent image of MMP-1 protein (visualized with RITC). Arrowheads, colocalization of MMP-1 protein and FLAG antigen; *microspheres. Original magnification: (**A** and **B**) ×200; (**C**) ×100. Scale bars: 50 μm.

TABLE 1. SERUM BIOCHEMICAL PARAMETERS OF MICE PREADMINISTERED GELATIN MICROSPHERES INCORPORATING pCMV-MMP OR OTHER AGENTS INTO RENAL SUBCAPSULE AFTER STZ INJECTION[a]

	Blood glucose[b] *(mg/dL)*	*BUN (mg/dL)*	*Cre*[c] *(mg/dL)*
Untreated (control)	203.3 ± 7.6[d]	21.5 ± 2.2	0.1 ± 0.0
STZ-injected group			
PBS	590.0 ± 165.8	27.3 ± 4.7	0.6 ± 0.1
Gelatin microspheres	508.3 ± 42.5	23.7 ± 2.1	0.6 ± 0.1
Free pCMV-MMP	588.3 ± 119.5	20.9 ± 5.0	0.5 ± 0.2
Gelatin microspheres incorporating pCMV-MMP	543.3 ± 178.5	19.9 ± 3.3[e]	0.5 ± 0.2

[a]Per site, 50 μg of pCMV-MMP.
[b]Blood glucose was measured 21 days after STZ injection.
[c]Blood urea nitrogen and serum creatinine were measured 28 days after STZ injection.
[d]Mean ± SD.
[e]$p < 0.05$; significant against the blood urea nitrogen of PBS-administered mice 28 days after STZ injection.

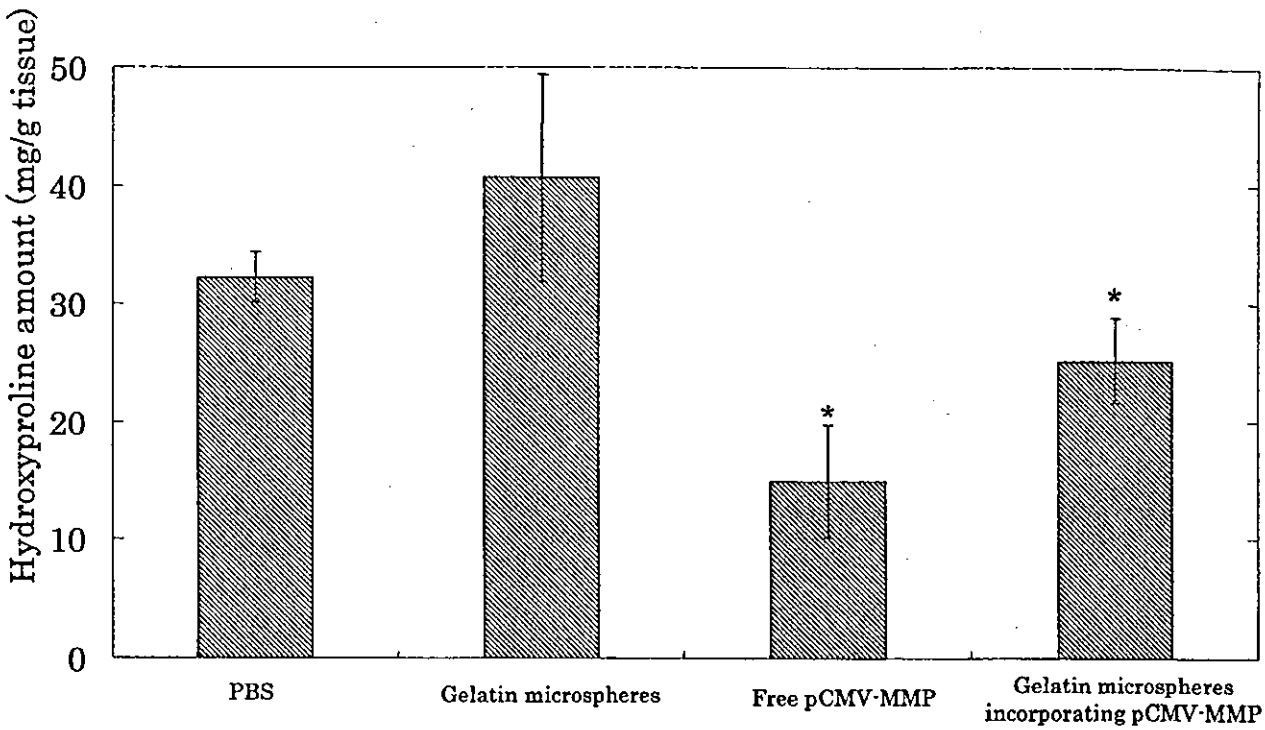

FIG. 4. Renal hydroxyproline amounts in mice preadministered gelatin microspheres incorporating pCMV-MMP or other agents into the renal subcapsule 28 days after STZ injection (50 μg of pCMV-MMP per site). Hydroxyproline amount was significantly reduced in mice preadministered microspheres incorporating pCMV-MMP and free pCMV-MMP. $*p < 0.05$; significant against the hydroxyproline amount in PBS-administered mouse group.

scaffolds, and growth factors.[22] However, destructive fibrosis can be interpreted as decreased ECM, where a scaffold suitable for natural tissue regeneration is denatured and excessive collagen is accumulated. Thus, it is possible from the biological function of MMP-1 that this substance acts on excess collagen to digest and convert the diseased and fibrotic ECM to a flexible scaffold, enabling cells to proliferate and to differentiate to induce tissue regeneration. Because systemic administration would not be clinically desirable and excessive amounts may cause other unfavorable effects, drug delivery system (DDS) technology to the local site is indispensable.

The present study demonstrated that cationized gelatin hydrogels were useful for the local controlled release of plasmid DNA (Figs. 1 and 2). This system is based on gene delivery by nonviral vectors, such as cationized liposome and polymers. Viral or virally derived vectors, such as adenovirus or retrovirus, transfect DNA with high efficiency, but their use is limited as a result of several concerns. They involve immunogenicity, cytotoxicity, the possibility of mutanogenesis, some technological difficulties, and the cost of viral vectors.[23] Moreover, reports claim the risk of germ line changes.[24] These phenomena suggest to us that viral vectors sometimes act beyond proper control. Our sustained release system of plasmid DNA, on the other hand, has several advantages. When the hydrogel is degraded to generate water-soluble and degraded fragments of cationized gelatin, plasmid DNA molecules are released from the hydrogels in complex with degraded gelatin fragments. Because the plasmid DNA released is complexed with cationized gelatin, this complexation enhances the transfection of plasmid DNA into cells. Expression at the targeted site can be regulated by changing the dose of plasmid DNA and the hydrogel degradability, which is controllable by regulating the cross-linking extent of the hydrogel.[13]

Sustained release of plasmid DNA at a local site is effective in enhancing the level of gene expression as well as in prolonging the expressed time period (Fig. 2). Immunofluorescence microscopic observation indicated that MMP-1 protein was generated in renal tissue next to the microsphere injection site (Fig. 3). It is not clear which type of mouse kidney cells received the transgene and expressed MMP-1, nor to what extent these cells produced MMP-1, but these results indicate that microspheres incorporating pCMV-MMP functioned effectively inside the mouse kidney even though they were injected into the renal subcapsule.

Hydroxyproline determination revealed that microspheres incorporating pCMV-MMP and free plasmid DNA had similar effects (Fig. 4), while histological and biochemical examinations exhibited a significant im-

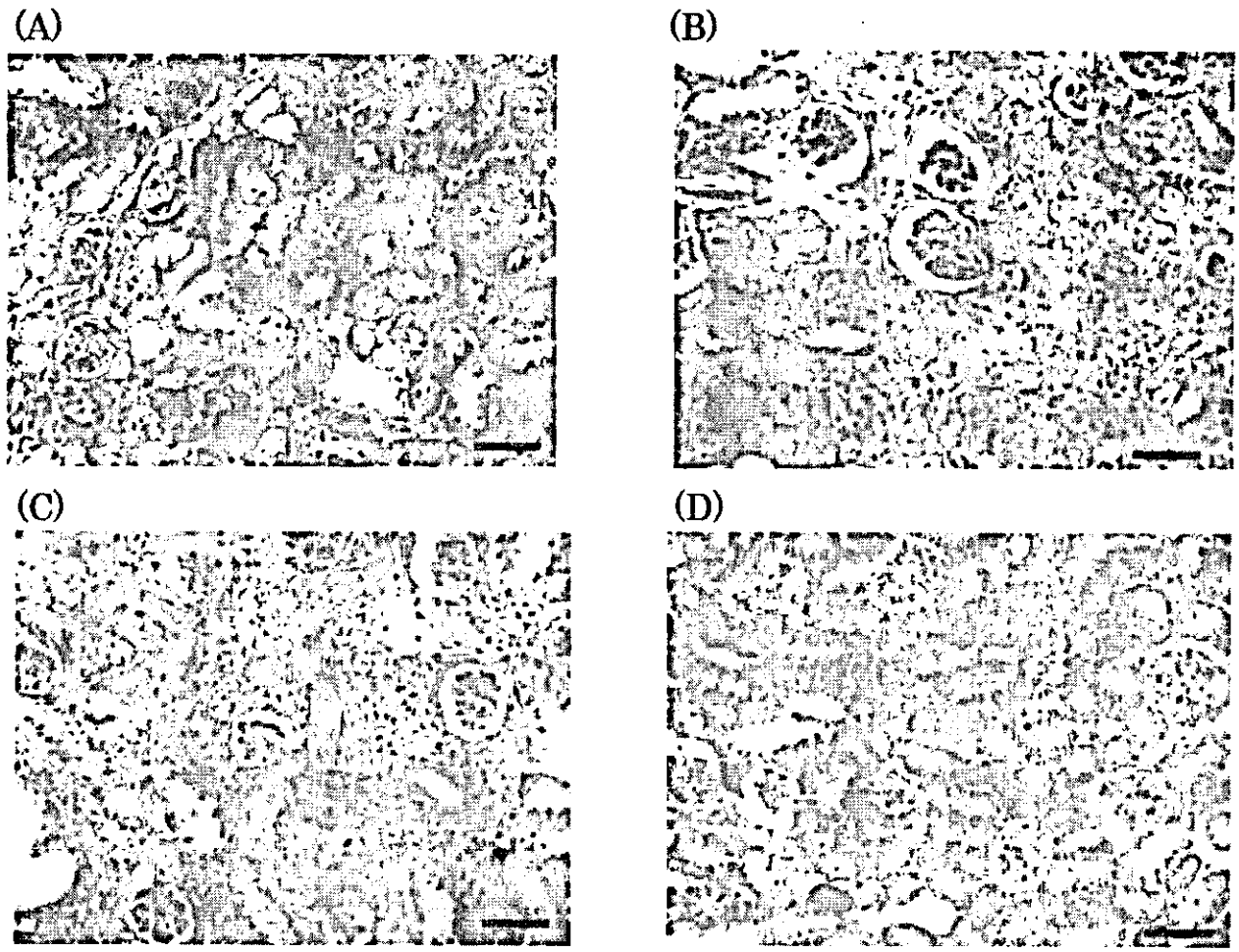

FIG. 5. Renal histological sections of mice preadministered gelatin microspheres incorporating pCMV-MMP or other agents into the renal subcapsule 28 days after STZ injection: (A) PBS, (B) gelatin microspheres, (C) free pCMV-MMP (50 μg/site), and (D) gelatin microspheres incorporating pCMV-MMP (50 μg/site). Masson trichrome stain; original magnification, ×200.

provement in renal fibrosis and renal function by microspheres incorporating pCMV-MMP. This difference may be explained in terms of a characteristic trait of the assay system. Histological sections may not reflect the total amount of collagen, because two-dimensional analyses inevitably are limited in estimating a three-dimensional property, while hydroxyproline determination does not display the distribution of fibrous tissue. Biochemical parameters are, however, closely related to the clinical outcome of any therapeutical approach.[25] The final goal of this present prophylactic trial was the preservation of renal function. Therefore, we can say with fair certainty that the biochemical results, indicating the prophylactic feasibility of microspheres incorporating plasmid DNA, suggested the successful improvement of renal function.

When all the data are taken together, the suppression of collagen type I synthesis and blood urea nitrogen in mice preadministered gelatin microspheres incorporating pCMV-MMP clearly indicates that inhibition of fibrogenesis paved the way for conservation of renal function. In general, injured tissue is gradually repaired by the excessive formation of fibrous tissues (scar formation), which eventually suppresses natural tissue regeneration. If such fibrosis could be suppressed or if the hypertrophically formed tissue could be excluded, it is expected that natural tissue could be regenerated. MMP-1 digestion enables the fibrotic tissue to convert to such a state that the natural process of tissue regeneration can readily be induced. This strategy is new and different from the "surgical" tissue engineering in which tissue regeneration is induced by surgically adding the cells, scaffold, and growth factor. This can be defined as "internal medicine" tissue engineering; the approach will not only contribute to complete cure for fibrotic diseases but also permit natural tissue regeneration thereafter.[22] In this approach, natural healing capability is induced by removing the pathogenic cause from the site where regeneration is expected. This approach would be applicable to a variety of enzymes and genes other than MMP-1.

REFERENCES

1. Bohle, A., Wehrmann, M., Bogenschutz, O., Batz, C., Muller, C.A., and Muller, G.A. The pathogenesis of chronic renal failure in diabetic nephropathy: Investigation of 488 cases of diabetic glomerulosclerosis. Pathol. Res. Pract. **187,** 251, 1991.
2. Eddy, A.A. Molecular insights into renal interstitial fibrosis. J. Am. Soc. Nephrol. **7,** 2495, 1996.
3. Remuzzi, G., and Bertani, T. Pathophysiology of progressive nephropathies. N. Engl. J. Med. **339,** 1448, 1998.
4. Nath, K.A. The tubulointerstitium in progressive renal disease. Kidney Int. **54,** 992, 1998.
5. Wang, S., Denichilo, M., Brubaker, C., and Hirschberg, R. Connective tissue growth factor in tubulointerstitial injury of diabetic nephropathy. Kidney Int. **60,** 96, 2001.
6. Border, W., and Noble, N. TGF-β in kidney disease: A target for gene therapy. Kidney Int. **51,** 1388, 1997.
7. Schena, P., Gesualdo, L., Grandiliano, G., and Montinaro, V. Progression of renal damage in human glomerulonephitides: Is there a sleight of hand in the winning game? Kidney Int. **52,** 1439, 1997.
8. Franklin, T. Therapeutic approaches to organ fibrosis. Int. J. Biochem. Cell Biol. **29,** 79, 1997.
9. Mizuno, S., Matsumoto, K., Kurosawa, T., Mizuno-Horikawa, Y., and Nakamura, T. Reciprocal balance of hepatocyte growth factor and transforming growth factor-β_1 in renal fibrosis in mice. Kidney Int. **57,** 937, 2000.
10. Iimuro, Y., Nishio, T., and Yamaoka, Y. Gene transfer of MMP-1 for treatment of established fibrosis. BIO Clin. (Tokyo) **16,** 330, 2001.
11. Garcia-Banuelos, J., Siller-Lopez, F., Miranda, A., Aguilar, L.K., Aguilar-Cordova, E., and Armendariz-Borunda, J. Cirrhotic rat livers with extensive fibrosis can be safely transduced with clinical-grade adenoviral vectors: Evidence of cirrhosis reversion. Gene Ther. **9,** 127, 2002.
12. Luo, D., and Saltzman, W.M. Synthetic DNA delivery systems. Nat. Biotechnol. **18,** 33, 2000.
13. Fukunaka, Y., Iwanaga, K., Morimoto, K., Kakemi, M., and Tabata, Y. Controlled release of plasmid DNA from cationized gelatin hydrogels based on hydrogel degradation. J. Control. Release **80,** 333, 2002.
14. Katoh, M., Ohmachi, Y., Kurosawa, Y., Yoneda, H., Tanaka, N., and Narita, H. Effects of imidapril and captopril on streptozotocin-induced diabetic nephropathy in mice. Eur. J. Pharmacol. **398,** 381, 2000.
15. Snyder, S.L., and Sobocinski, P.A. An improved 2,4,6-trinitro-benzenesulfonic acid method for the determination of amines. Anal. Biochem. **64,** 284, 1975.
16. Tabata, Y., Hijikata, S., Muniruzzaman, M., and Ikada, Y. Neovascularization effect of biodegradable gelatin microspheres incorporating basic fibroblast growth factor. J. Biomater. Sci. Polym. Ed. **10,** 79, 1999.
17. Rosevear, J.W., Pfaff, K.J., Service, F.J., Molnar, G.D., and Ackerman, E. Glucose oxidase method for continuous automated blood glucose determination. Clin. Chem. **15,** 680, 1969.
18. Kivirikko, K.I., Laitinen, O., and Prockop, D.J. Modifications of a specific assay for hydroxyproline in urine. Anal. Biochem. **19,** 249, 1967.
19. Chambers, A.F., and Matrisian, L.A. Changing views on the role of matrix metalloproteinases in metastasis. J. Natl. Cancer Inst. **89,** 1260, 1997.
20. Parsons, S.L., Watson, S.A., Brown, P.D., Collins, H.M., and Steele, R.J.C. Matrix metalloproteinases. Br. J. Surg. **84,** 160, 1997.
21. Curran, S., and Murray, G.I. Matrix metalloproteinases in tumor invasion and metastasis. J. Pathol. **189,** 300, 1999.
22. Tabata, Y. Recent progress in tissue engineering. Drug Discov. Today **6,** 483, 2001.
23. Romano, G., Michell, P., Pacilio, C., and Giordano, A. Latest developments in gene transfer technology: Achievements, perspectives, and controversies over therapeutic applications. Stem Cells **18,** 19, 2000.
24. Boyce, N. Trial halted after gene shows up in semen. Nature **414,** 677, 2001.
25. Yu, L., Noble, N.A., and Border, W.A. Therapeutic strategies to halt renal fibrosis. Curr. Opin. Pharmacol. **2,** 177, 2002.

Address reprint requests to:
Yasuhiko Tabata, Ph.D., D.Med.Sci., D.Pharm.
Department of Biomaterials
Institute for Frontier Medical Sciences
Kyoto University
53 Kawara-cho Shogoin, Sakyo-ku
Kyoto 606-8507, Japan

E-mail: yasuhiko@frontier.kyoto-u.ac.jp

JOURNAL OF MATERIALS SCIENCE: MATERIALS IN MEDICINE 14 (2003) 973–978

Surface modification of a porous hydroxyapatite to promote bonded polymer coatings

ATSUSHI MATSUDA[1]*, TSUTOMU FURUZONO[2], DOMINIC WALSH[3], AKIO KISHIDA[2], JUNZO TANAKA[1]
[1]*Biomaterials Center, National Institute for Materials Science, 1-1 Namiki, Tsukuba, Ibaraki 305-0044, Japan*
[2]*Department of Bioengineering, National Cardiovascular Center Research Institute, 5-7-1 Fujishiro-dai, Suita, Osaka 565-8565, Japan*
[3]*School of Chemistry, University of Bristol, Cantock Close, Bristol BS8 1TS, UK*
Email: Matsuda.atsushi@nims.go.jp

Porous hydroxyapatite (Hap) blocks were sintered at several temperatures and methyl methacrylate (MMA) grafted onto the surface in a 2-step heterogeneous system as a model example for surface modification. First, sintered porous Hap was modified with 2-methacryloyloxyethylene isocyanate (MOI) monomer in anhydrous dimethyl sulfoxide using di-*n*-butyltin (IV) dilaurate as a catalyst and hydroquinone as an inhibitor. Amount of the introduction of MOI monomer on porous Hap was 1.62 wt% at sintered temperature 800 °C, 0.68 wt% at it of 1000 °C, and 0.59 wt% at it of 1200 °C. Scanning electron microscopy (SEM) showed that porous Hap pore size and shape before and after MOI treatment were unchanged. Second, graft polymerization with MMA through the vinyl bond on porous Hap was conducted using α,α′-azobis isobutyronitrile (AIBN) as an initiator. Amount of Grafted PMMA on the MOI modified porous Hap was 2.84 wt% at sintered temperature of 800 °C, 6.97 wt% at it of 1000 °C, and 6.27 wt% at it of 1200 °C. MOI-modified and PMMA-grafted porous Hap were characterized using Fourier transform infrared (FT-IR) spectroscopy. The compressive strength of sintered porous Hap with grafted PMMA increased about 2.7–6.7 times compared to intact porous Hap. This 2-step surface modification on porous Hap is widely applicable to graft polymerization with vinyl polymer and conjugation with a protein or an oligopeptide, such as growth factor or an adhesion molecule, to improve Hap mechanical properties and functionality.

1. Introduction

Hydroxyapatite (Hap) has been used in medical applications such as bone implant materials [1–3]. Porous natural corals have also been used because the macroporosity of these materials promotes osteoconductivity and resorption *in vivo*. Walsh *et al.* reported synthesizing unique porous Hap with continuous cavities formed by a foaming calcium phosphate preparation [4, 5]. Porous Hap was applicable for graft cartridges in maxillofacial surgery [6] as alveolar ridge augments and as bone defect filler [7]. Mechanical strength, or cell adhesion and tissue migration on porous Hap, may be limited by its crystallinity, or surface composition and morphology [8–12]. The use of Hap in medical implants would greatly increase if surface modification by an organic compound could improve its mechanical strength or functionality of cell adhesion or multiplication.

Composite preparation of organic materials with Hap has involved the use of coupling agents, such as silanes [13–15], zirconyl salts [16], and polyacid [17], and the introduction of a chemical linkage to octacalcium phosphate by coprecipitation [18, 19]. As is well known, organic compounds with isocyanate groups react readily with Hap surface hydroxyl groups [20].

This paper details a novel 2-step surface modification with an organic compound that improves porous Hap mechanical properties and functionality. We chose poly methyl methacrylate (PMMA) as a typical example for porous Hap surface modification. PMMA is a common polymer used as bone cement for fixing total hip prostheses [15, 18, 19, 21] to give suitable mechanical properties to the material. Initially, 2-methacryloyloxyethylene isocyanate (MOI) possessing a vinyl polymerizable double bond and a reactive isocyanate group at both ends of the compound is reacted with a hydroxyl group of Hap to introduce vinyl groups, applicable as initiation points for grafting PMMA onto porous Hap. We then studied reaction kinetics and the effect on porous Hap shape and microstructure.

*Author to whom all correspondence should be addressed.

0957–4530

2. Materials and methods

2.1. Materials

The following were used without further purification: calcium hydrogen phosphate dihydrate ($CaHPO_4 \cdot 2H_2O$) and calcium bis(dihydrogen phosphate) monohydrate ($Ca(H_2PO_4)_2 \cdot H_2O$, MCPM) (Wako Pure Chemical Industries, Ltd., Osaka, Japan); calcium carbonate ($CaCO_3$) (Kanto Chemical Co., Inc., Tokyo, Japan); and MOI monomer donated by Showa Denko Co. (Tokyo, Japan). The solvent dimethyl sulfoxide dehydrate (DMSO), the catalyst di-*n*-butyltin (IV) dilaurate, the inhibitor hydroquinone, and the solvent *N,N'*-dimethyl formamide dehydrate (DMF) were purchased from Wako Pure Chemical Industries, Ltd. Methyl methacrylate (MMA) was purchased from Wako Pure Chemical Industries, Ltd., and distilled in a vacuum. The initiator α,α'-azobis isobutyronitrile (AIBN) was purchased from Wako Pure Chemical Industries, Ltd., and recrystallized from ethanol.

2.2. Measurements

Porous Hap was characterized by X-ray diffraction (XRD) (Philips PW1729 X-ray diffractometer, The Netherlands) with Ni-filtered Cu Kα radiation (40 kV, 50 mA). JCPDS-PDF card 9-432 was used for XRD reference. We used scanning electron microscopy (SEM, Model EDSEM, JEOL, Tokyo, Japan) at 10 kV acceleration voltage to observe tungsten-coated samples of intact porous Hap and its MOI composites. Infrared spectra (Perkin-Elmer FT-IR Spectrometer Spectrum 2000, USA) were recorded from 4000–500 cm^{-1} using KBr discs. The amount of MOI and grafted PMMA on porous Hap was determined using thermogravimetry-differential thermal analysis (TG-DTA Rigaku Thermo plus TG8120, Japan). About 10 mg of samples were heated to 1200 °C at the heating rate of 20 °C/min. Compressive strength (Texture Analyzer Stable Micro Systems® TA-XT2i, UK) was measured on 10 mm × 20 mm cylindrical blocks (5) of intact porous Hap and PMMA-grafted porous Hap. Titration was used to determine the amount of MOI added to porous Hap samples as described elsewhere [24–26].

2.3. Chemical modification by MOI monomer

Porous Hap was prepared using a modification of that reported by Walsh *et al.* [4, 5]. Briefly, equimolar tetracalcium phosphate monoxide ($Ca_4(PO_4)_2O$, TCPM), $CaCO_3$, and MCPM were thoroughly mixed and 0.01 N HCl aqueous solution was added to 1 ml against 1 mg of mixed powder. The effervescing mixture was then rapidly mixed in a pestle and mortar before being packed into cylindrical molds. The porous cement block was then dried at room temperature for 24 h before soaking in 10^{-5} N NaOH aqueous solution at 37 °C for 3 days followed by air drying. A porous Hap cylindrical block 10 mm × 20 mm was prepared to cut the cylinders and modified with MOI monomer in a heterogeneous system. Porous Hap was dried for 24 h at 120 °C before use. We immersed 20 pieces of dried porous Hap in 49 ml anhydrous DMSO under nitrogen, and added 1.5 ml of MOI monomer and 0.05 g of di-*n*-butyltin (IV) dilaurate to an anhydrous system containing 150 ppm of hydroquinone. The reaction system was kept at 60 °C for 3, 6, 12, and 24 h. Chemically modified porous Hap was successively washed with DMSO and methanol to remove unreacted reagents. MOI-modified samples were dried at room temperature in a vacuum oven for 24 h.

2.4. Graft polymerization with PMMA

PMMA was grafted via vinyl groups onto porous Hap using AIBN as an initiator; 60 mmol of MMA and 1.0 mol % of AIBN were dissolved in 10 ml of anhydrous DMF. Six MOI-modified porous Hap blocks were immersed in the MMA monomer solution in a 40 ml glass bottle. Graft polymerization was achieved in a nitrogen atmosphere at 60 °C for 24 h. PMMA-grafted porous Hap was copiously washed three times with DMF followed by ethanol washing twice to remove ungrafted homopolymer, and the block was then dried under reduced pressure for 24 h.

3. Results and discussion

3.1. Porous hydroxyapatite

XRD profiles of porous Hap cement unsintered and sintered at 800, 1000, and 1200 °C are shown in Fig. 1(a)–(d). Initially, the reaction between MCPM and $CaCO_3$ formed brushite ($CaHPO_4 \cdot 2H_2O$, DCPD) and simultaneously produced CO_2 gas making interconnecting holes in the bulk [5]. After DCPD and TCPM

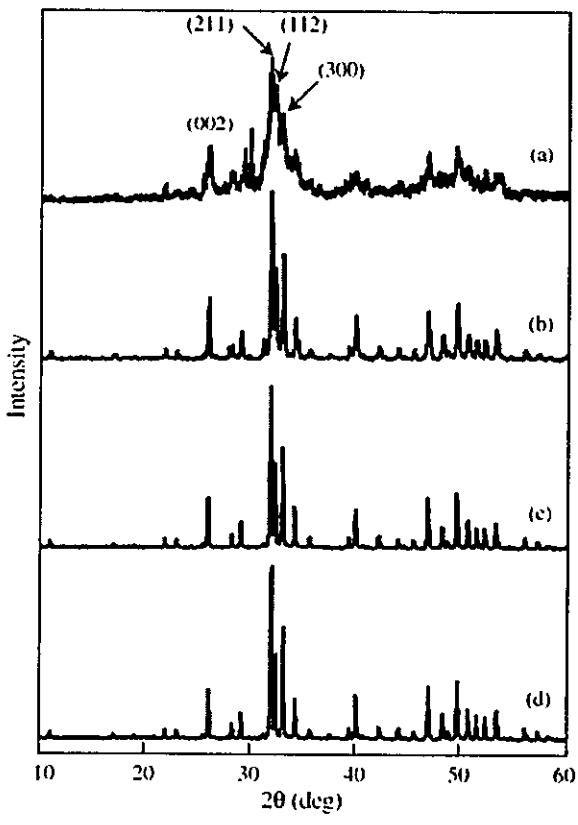

Figure 1 XRD profiles of porous Hap; (a) unsintered; sintered at (b) 800 °C, (c) 1000 °C, and (d) 1200 °C.

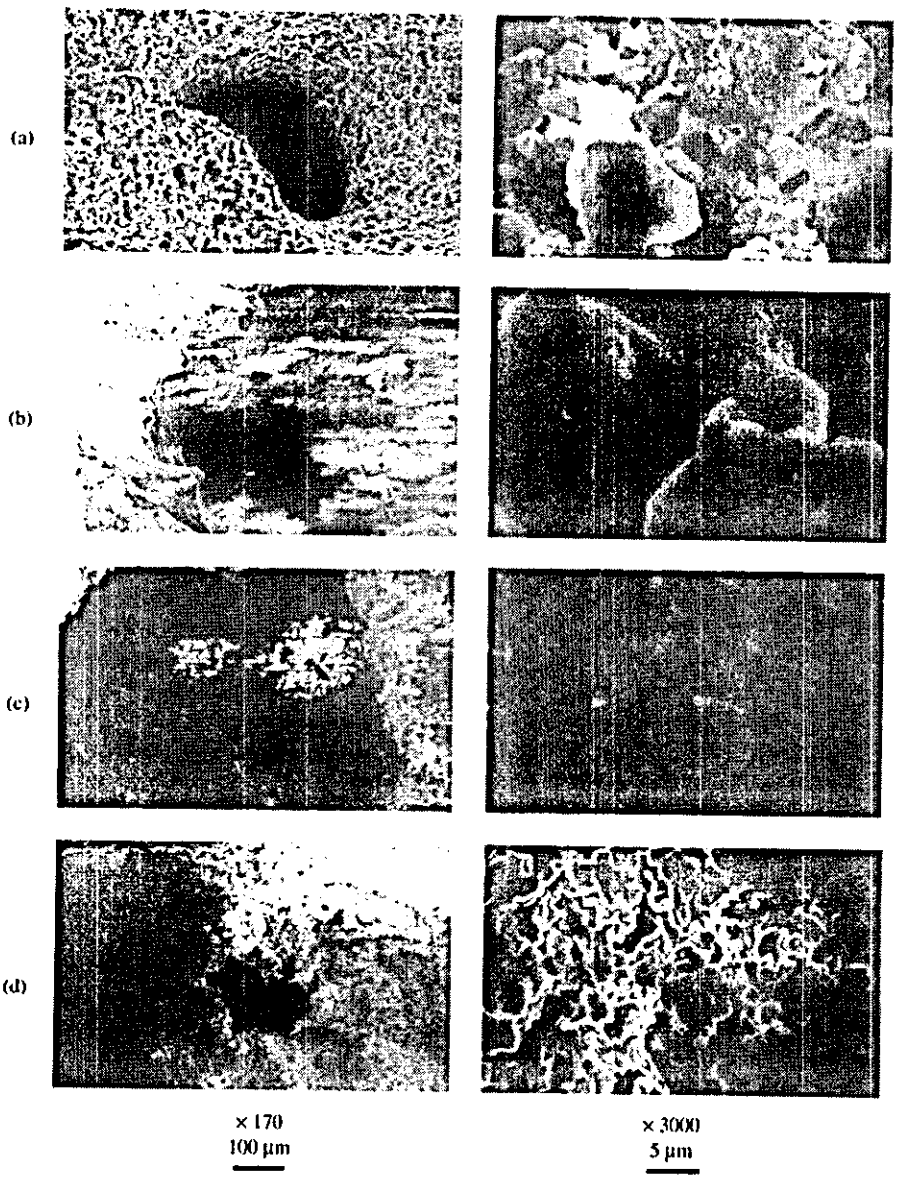

Figure 2 SEM micrographs of porous Hap; (a) unsintered; sintered at (b) 800 °C, (c) 1000 °C, and (d) 1200 °C.

were reacted in the NaOH solution for 3 days, the cement converted to Hap (Fig. 1(a)). With increasing sintering temperature, Hap peaks at (0 0 2), (2 1 1), (1 1 2), and (3 0 0) become sharper due to increasing crystallinity.

Fig. 2 shows a SEM micrograph of samples of macropores and microstructures. The macropore size decreased from 200 to 100 nm with increasing sintering temperature. Hap crystal growth by sintering changed pore size and crystal shape. The microstructure of porous Hap sintered at 800 °C showed a microrugged structure. Samples sintered at 1000 and 1200 °C, however, had a smooth structure. Yubao *et al.* [22] reported that calcium-deficient apatite particles melt about these temperatures, so this change in porous Hap crystal microstructure may be caused by Hap crystal melting during heating from 800 to 1000 °C.

3.2. Introduction of vinyl groups

Porous Hap was chemically modified with MOI monomer in an anhydrous system. Di-*n*-butyltin (IV) dilaurate as a catalyst effectively promoted the reaction between the isocyanate group and hydroxyl groups [23]. We plotted the amount of MOI monomer on porous Hap against reaction time at 60 °C (solid symbols, Fig. 3) determined using TG-DTA to calculate weight loss between room temperature and 600 °C. Open symbols show the amount of MOI monomer on porous Hap calculated by titration to determine the amount of vinyl groups contributing to polymerization [24–26].

It was clear that the polymerization-reaction of MOI by heating during the modification-reaction of the MOI monomer on/in the porous Hap did not occur because the amounts to MOI calculated through the TG-DTA and the titration for 24 h of reaction time took almost same value. MOI monomer added for a 24 h reaction with porous Hap sintered was calculated as 0.11 mmol/g at 800 °C, 0.044 mmol/g at 1000 °C, and 0.038 mmol/g at 1200 °C. In nonsintered Hap powder (BET-specific surface area of 66 m^2/g), Liu *et al.* reported that the amount modified with MOI monomer increased with increasing reaction time, finally reaching equilibrium of about 0.7 mmol/g in both reaction conditions at 50 °C/20 h and 70 °C/12 h [20]. The difference in reaction kinetics between porous

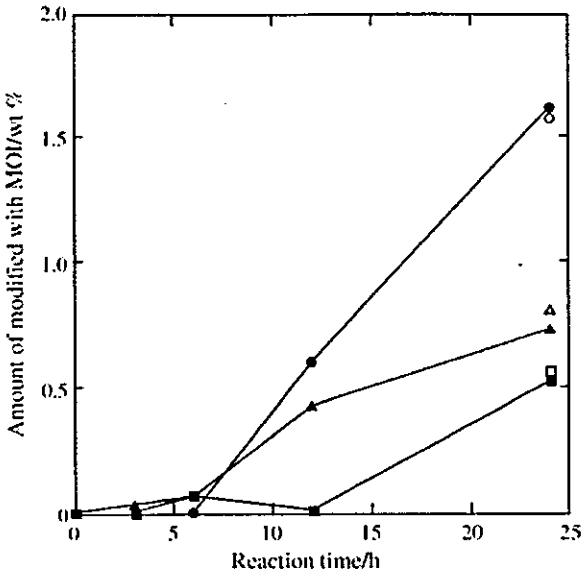

Figure 3 Weight gain of MOI monomer on porous Hap as a function of reaction time; sintered at (●) 800 °C, (▲) 1000 °C, and (■) 1200 °C. Open symbols were determined by titration.

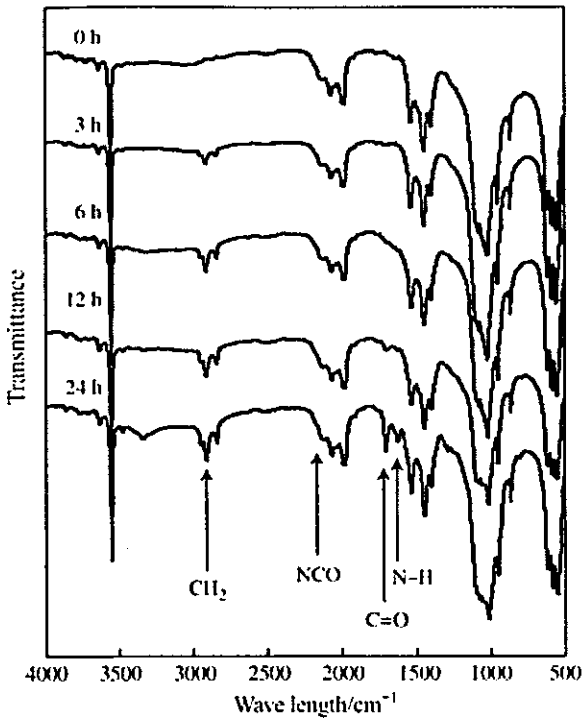

Figure 4 FT-IR spectra of MOI-modified porous Hap sintered at 800 °C. FT-IR spectra of MOI-modified porous Hap sintered at 1000 and 1200 °C were almost identical.

Hap and Hap powder is considered due to the restriction of MOI monomer diffusion to the inside of porous Hap and because the surface area of porous Hap able to react with MOI monomer was much less compared to Hap powder.

In FT-IR spectra of MOI-modified porous Hap sintered at 800 °C (Fig. 4), absorption at 2960 cm^{-1} is attributable to the stretching vibration of C–H, which increased with increasing MOI monomer on porous Hap. The presence of the deformation vibration of the amide N–H peak at 1660 cm^{-1} and of the stretching vibration of the ester C=O peak at 1730 cm^{-1} indicated that MOI monomer and porous Hap were coupled by covalent linkage, the peak attributed to the isocyanate group (–NCO) was clear at 2270 cm^{-1} in the spectrum of the MOI monomer [27]. The isocyanate group peak completely disappeared after MOI monomer was added to porous Hap (Fig. 4), indicating the isocyanate group of the MOI monomer reacted completely with Hap hydroxyl groups under our reaction conditions. The peak of about 1450 cm^{-1} corresponded to ν_3CO_2, the broad band over 1000–1150 cm^{-1} corresponded to ν_3PO_4, the peak of about 630 cm^{-1} corresponded to δOH, and the peaks of about 570 and 600 cm^{-1} to the ν_4PO_4, indicating Hap formation.

Fig. 5 shows SEM observations of MOI-modified porous Hap at low and high magnification. Macro- and microchannels of porous Hap were unchanged by MOI monomer modification compared to Fig. 1, implying that MOI monomer was coated as a thin layer on porous Hap.

3.3. Graft polymerization with MMA

MMA was graft-polymerized on porous Hap through vinyl groups in the MOI monomer using AIBN as a polymerization initiator. We determined the amount of PMMA grafting on MOI-modified porous Hap using TG-DTA (Table I). When graft polymerization with MMA was done using un-modified porous Hap, the amount of graft polymerization of PMMA was zero after washing with DMF. Table I shows that weight gain refers only to the amount of grafting PMMA on porous Hap attached by covalent bonding. MMA grafted on porous Hap sintered at 800 °C was significantly lower compared to that sintered at 1000 and 1200 °C, although MOI modification on porous Hap sintered was significantly higher. There might be two reasons to explain this phenomenon: first, MMA monomer is difficult to diffuse and react the vinyl groups in the micro-cavity of the 800 °C sintered porous Hap, since it has the micro-rugged structure as shown in Fig. 5. Second, sintered porous Hap at 800 °C has too small space that limits the growth reaction of the PMMA graft chain.

FT-IR spectra of PMMA homopolymer and PMMA-grafted porous Hap are shown in Fig. 6. Compared with

TABLE I Weight% of add-on MOI, grafting PMMA, and compressive strength of porous Hap

Sintered temperature/°C	MOI add-on/ wt%	Grafting polymer (PMMA)/wt%	Compressive strength at intact porous Hap/MPa	Compressive strength at PMMA grafted porous Hap/MPa
800	1.62	2.84	1.54	10.3
1000	0.68	6.97	3.24	21.2
1200	0.59	6.27	17.3	47.1

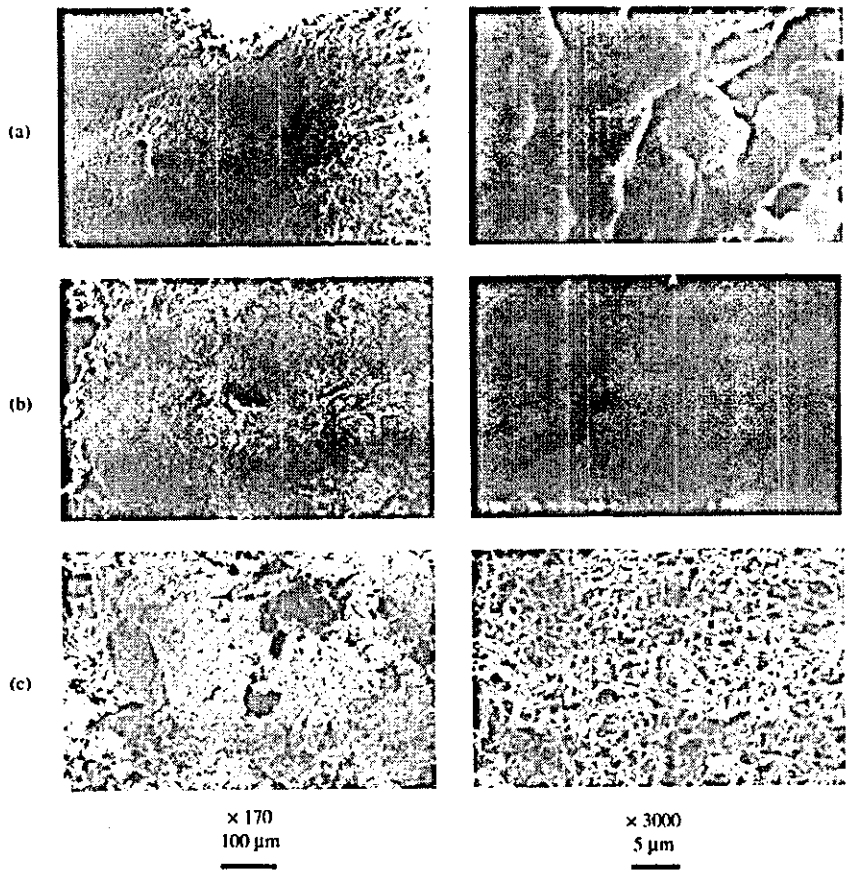

Figure 5 SEM micrographs of MOI-modified porous Hap; sintered at (a) 800 °C, (b) 1000 °C, and (c) 1200 °C.

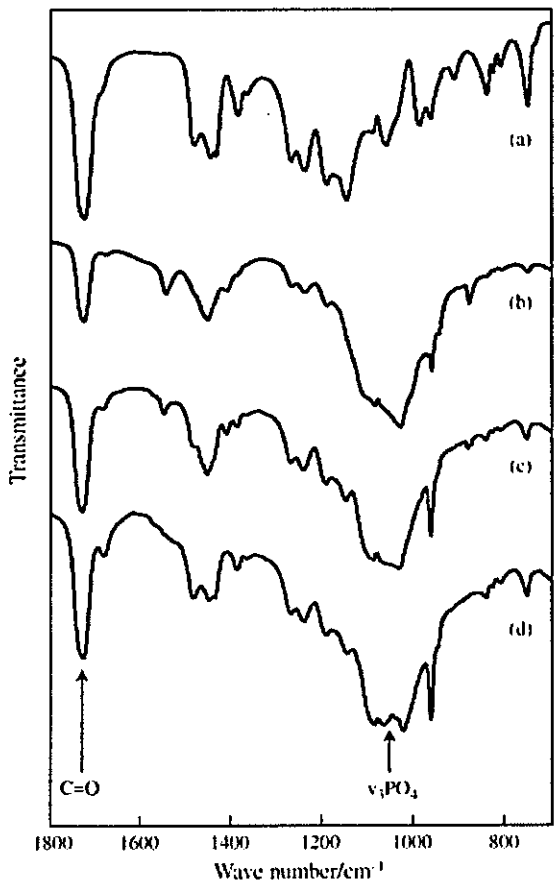

Figure 6 FT-IR spectra of PMMA-grafted porous Hap; (a) PMMA homopolymer; sintered at (b) 800 °C, (c) 1000 °C, and (d) 1200 °C.

Fig. 4, absorption at about 1730 cm^{-1} attributed to the ester C=O peak increased with increasing PMMA grafting, clearly showing that PMMA was grafted successfully on porous Hap. The ratio of the peak strength between the C=O and the PO_4 band of porous Hap sintered at 800 °C (Fig. 6(b)) indicates that the amount of grafted PMMA was less than that of samples sintered at 1000 (c) and 1200 °C (d), which agreed well with PMMA grafted on Hap (Table I).

The compressive strength of intact porous Hap sintered at 800, 1000, and 1200 °C (Table I) increased with increasing sintering temperature, because the crystal growth of porous Hap and apparent density of porous Hap by melting with increasing the sintering temperature. The compressive strength of porous Hap grafted with PMMA increased 4.5 times over the sintering temperature range compared to 11.2 times for uncoated porous Hap. Porous Hap strength thus increased dramatically with this surface modification. For porous Hap sintered at 800 °C, compressive strength increased 6.7 times that of uncoated Hap, even though the amount of PMMA was low. The compressive strength of PMMA-grafted porous Hap sintered at 1000 °C was roughly half that sintered at 1200 °C, although the amount of PMMA grafted on porous Hap sintered at 1000 and 1200 °C was similar. These results indicate that compressive strength could be greatly affected by grafting a thin layer of PMMA on Hap, so we can synthesize porous Hap having desired mechanical properties over a wide range from 1.5 to 47 MPa by controlling the sintering temperature of Hap blocks to be coated and the amount of PMMA then to be grafted.

4. Conclusions

We developed a way to modify the porous Hap surface through an introduced functional group attached by covalent linkage. PMMA provided porous Hap with mechanical and biostable properties through bonding to a vinyl group coupled on porous Hap. PMMA was used as an example polymer for interaction with the Hap surface modified by MOI. This two-step surface modification of Hap is widely applicable to graft polymerization with a vinyl polymer and conjugation with biomolecules, such as proteins or oligopeptides [28], to improve Hap mechanical properties and functionality. We are now developing a 3-dimensional cell-culture vessel and biomolecule separator using porous Hap cartridges grafted with vinyl- and biopolymers.

References

1. I. SOTEN and G. A. OZIN, *J. Mater. Chem.* 9(3) (1999) 703.
2. L. C. CHOW, *J. Ceram. Soc. Japan.* 99(10) (1991) 954.
3. M. KIKUCHI, S. ITOH, S. ICHINOSE, K. SHINOMIYA and J. TANAKA, *Biomaterials* **22** (2001) 1705.
4. D. WALSH and S. MANN, in "Handbook of Biomimetics", vol. S6, edited by Y. Osada (NTS Inc., Tokyo, Japan, 2000) 59, Chapter 1.
5. D. WALSH, T. FURUZONO and J. TANAKA, *Biomaterials* **22** (2001) 1205.
6. P. YLINEN, M. RAEKALLIO, T. TOIVONEN, K. VIHTONEN and S. VAINONPAA, *J. Oral Maxillofac. Surg.* **49** (1991) 1191.
7. R. W. BUCHOLZ, A. CARLTO and R. HOLMES, *Clin. Orthop.* **240** (1989) 53.
8. T. M. CHU, D. G. ORTON, S. J. HOLLISTER, S. E. FEINBERG and J. W. HALLORAN, *Biomaterials* 23(5) (2002) 1283.
9. S. JOSCHEK, B. NIES, R. KROTZ and A. GOFERICH, *ibid.* **21**(16) (2000) 1645.
10. W. J. BIGHAM, P. STANLEY, J. M. CAHILL JR, R. W. CURRAN and A. C. PERRY, *Ophthal. Plast. Reconstr. Surg.* **15**(5) (1999) 317.
11. B. K. VAUGHN, A. V. LOMBARDI JR and T. H. MALLORY, *Semin. Arthoplasty.* 2(4) (1991) 309.
12. G. JIANG and D. SHI, *J. Biomed. Mater. Res.* **43**(1) (1998) 77.
13. A. M. P. DUPRAZ, J. R. DE WIJN, S. A. T. VAN DER MEER and K. DE GROOT, *ibid.* **30** (1996) 231.
14. K. NISHIZAWA, M. TORIYAMA, T. SUZUKI, Y. KAWAMOTO, Y. YOKUGAWA and F. NAGATA, *Chem. Soc. Jpn.* **1** (1995) 63.
15. J. C. BEHIRI, M. BRADEN, S. KHORASANI, D. WIWATTANADATE and W. BONFIELD, in "Bioceramics", vol. 4, edited by W. Bonfield, G. W. Hastings and K. E. Tanner (Elsevier Science, London, 1991) 301.
16. D. N. MISRA, *J. Dent. Res.* **12** (1985) 1405.
17. Q. LIU, J. R. DE WIJN, M. VAN TOLEDO, D. BAKKER and C. A. VAN BLITTERSWIJK, *J. Mater. Sci.: Mater. Med.* 7 (1996) 551.
18. V. DELPECH and A. LEBUGLE, *Clin. Mater.* 5 (1990) 209.
19. J. DANDURAND, V. DELPECH, A. LEBUGLE, A. LAMURE and C. LACABANNE, *J. Biomed. Mater. Res.* **24** (1990) 1377.
20. Q. LIU, J. R. DE WIJN and C. A. VAN BLITTERSWIJK, *ibid.* 40(3) (1998) 490.
21. R. LABELLA, M. BRADEN and S. DEB, *Biomaterials* **15** (1994) 1197.
22. L. YUBAO, C. P. A. T. KLEIN, J. DE WIJN and S. VAN DE MEER, *J. Mater. Sci.: Mater. Med.* 5 (1994) 263.
23. M. R. THOMAS, *J. Coat. Technol.* 55 (1983) 55.
24. A. BAYER, *Ann.* **245** (1888) 103.
25. H. MEYER, *Ber.* **28** (1895) 2965.
26. R. MEYER and E. HARTMANN, *ibid.* **38** (1905) 3956.
27. T. FURUZONO, K. ISHIHARA, N. NAKABAYASHI and Y. TAMADA, *Biomaterials.* **21** (2000) 327.
28. G. T. HERMANSON, "Bioconjugate Techniques" (Academic Press, Inc., New York, 1996).

Received 15 August 2002
and accepted 3 June 2003

ELSEVIER

Cardiovascular Research 58 (2003) 390–398

Cardiovascular Research

www.elsevier.com/locate/cardiores

Review

Post-natal endothelial progenitor cells for neovascularization in tissue regeneration

Haruchika Masuda[a,b,1], Takayuki Asahara[a,b,c,*]

[a]*Department of Physiology, Tokai University School of Medicine, Bohseidai, Isehara, Kanagawa 259-1193, Japan*
[b]*Research Center for Regenerative Medicine, Tokai University School of Medicine, Bohseidai, Isehara, Kanagawa 259-1193, Japan*
[c]*Division of Cardiovascular Research and Medicine, St Elizabeth's Medical Center, 736 Cambridge Street, Brighton, MA 02135-2997, USA*

Received 25 September 2002; accepted 15 November 2002

Abstract

The isolation of endothelial progenitor cells (EPCs) derived from bone marrow (BM) was an outstanding event in the recognition of 'de novo vessel formation' in adults occurring as physiological and pathological responses. The finding that EPCs home to sites of neovascularization and differentiate into endothelial cells (ECs) in situ is consistent with 'vasculogenesis', a critical paradigm well described for embryonic neovascularization, but proposed recently in adults in which a reservoir of stem or progenitor cells contributes to vascular organogenesis. EPCs have also been considered as therapeutic agents to supply the potent origin of neovascularization under pathological conditions. This review provides an update of EPC biology as well as highlighting their potential use for therapeutic regeneration.

Keywords: Experimental; Vasculature; Cellular; Circulatory physiology

1. Introduction

Tissue regeneration by somatic stem/progenitor cells has been recognized as a maintenance or recovery system of many organs in adult. The isolation and investigation of these somatic stem/progenitor cells has described how these cells contribute to postnatal organogenesis. On the basis of the regenerative potency, these stem/progenitor cells are expected to develop as a key strategy of therapeutic applications for the damaged organs.

Recently endothelial progenitor cells (EPCs) have been isolated from adult peripheral blood (PB). EPCs are considered to share common stem/progenitor cells with hematopoietic stem cells and have been shown to derive from bone marrow (BM) and to incorporate into foci of physiological or pathological neovascularization. The finding that EPCs home to sites of neovascularization and differentiate into endothelial cells (ECs) in situ is consistent with 'vasculogenesis', a critical paradigm well described for embryonic neovascularization, but recently proposed in adults in which a reservoir of stem/progenitor cells contributes to post-natal vascular organogenesis. The discovery of EPCs has therefore drastically changed our understanding of adult blood vessel formation. The following review provides an update of EPC biology as well as highlighting their potential utility for therapeutic vascular regeneration.

2. Post-natal neovascularization

Through the discovery of EPCs in PB [1,2], our understanding of post-natal neovascularization has been expanded from angiogenesis to angio/vasculogenesis. As previously described [3], post-natal neovascularization was

*Corresponding author. Present address: Division of Cardiovascular Research and Medicine, St Elizabeth's Medical Center, 736 Cambridge Street, Brighton, MA 02135-2997, USA. Tel.: +1-617-789-3156; fax: +1-617-779-6346.
E-mail addresses: harrymasuda@aol.com (H. Masuda), asa777@aol.com (T. Asahara).
[1]Tel./fax: +81-463-93-1121x2722.

Time for primary review 19 days.

0008-6363/03/$ – see front matter
doi:10.1016/S0008-6363(02)00785-X

originally recognized to be constituted by the mechanism of 'angiogenesis', which is neovessel formation, operated by in situ proliferation and migration of preexisting endothelial cells. However, the isolation of EPCs resulted in the addition of the new mechanism, 'vasculogenesis', which is de novo vessel formation by in situ incorporation, differentiation, migration, and/or proliferation of BM-derived EPCs [4] (Fig. 1). More recently, tissue specific stem/progenitor cells with the potency of differentiation into myocytes or ECs were isolated in skeletal muscle tissue of murine hindlimb, although the origin remains to be clarified [5]. This finding suggests that the origin of EPCs may not be limited to BM, e.g. tissue specific stem/progenitor cells possibly provide 'in situ EPCs' as other sources of EPCs than BM.

In the event of minor scale neovessel formation, i.e. slight wounds or burns, 'in situ preexisting ECs' causing post-natal angiogenesis may replicate and replace the existing cell population sufficiently, as ECs exhibit the ability for self-repair that preserves their proliferative activity. Neovascularization through differentiated ECs, however, is limited in terms of cellular life span (Hayflick limit) and their inability to incorporate into remote target sites. In the case of large scale tissue repair, such as patients who experienced acute vascular insult secondary to burns, coronary artery bypass grafting (CABG), or acute myocardial infarction [6,7], or in physiological cyclic organogenesis of endometrium [4], BM-derived or in situ EPC kinetics are activated under the influence of appropriate cytokines, hormones and/or growth factors through the autocrine, paracrine, and/or endocrine systems. Thus the contemporary view of tissue regeneration is that neighboring differentiated ECs are relied upon for vascular regeneration during a minor insult, whereas tissue specific or BM-derived stem/progenitor cells bearing EPCs/ECs are important when an emergent vascular regenerative process is required (Fig. 1).

3. Profiles of EPCs in adults

3.1. The evidence of circulating EPCs in adults

In the embryo, evidence suggests that hematopoietic stem cells (HSCs) and EPCs [8,9] are derived from a common precursor (hemangioblast) [10,11]. During embryonic development, multiple blood islands initially fuse to form a yolk sac capillary network [12], which provides the foundation for an arteriovenous vascular system that eventually forms following the onset of blood circulation [8]. The integral relationship between the cells which circulate in the vascular system (the blood cells) and those principally responsible for the vessels themselves (ECs) is suggested by their spatial orientation within the blood islands; those cells destined to generate hematopoietic cells are situated in the center of the blood island (HSCs) while EPCs or angioblasts are located at the periphery of the blood islands. In addition to this arrangement, HSCs and EPCs share common antigens, including CD34, Vascular

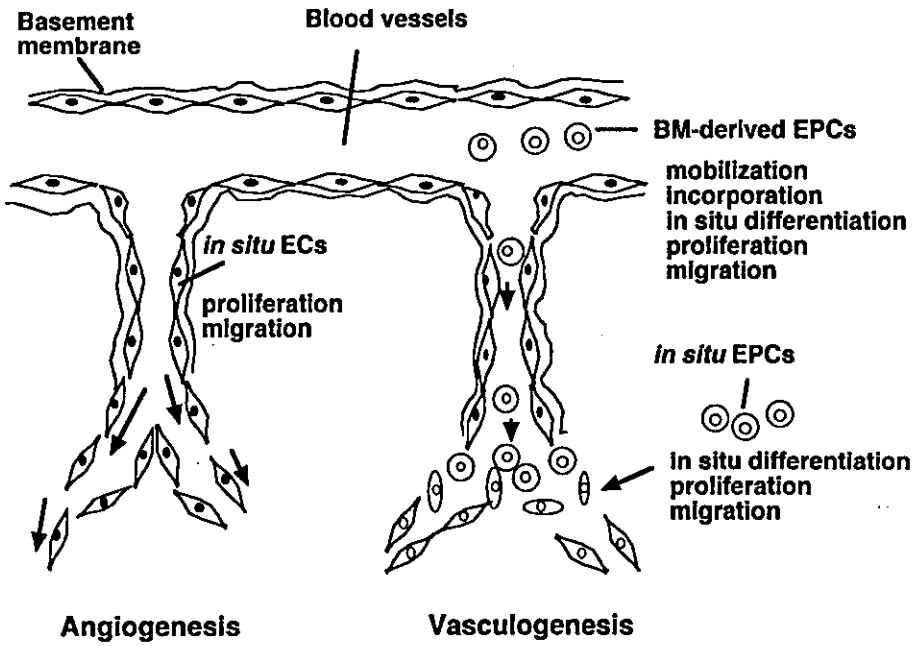

Fig. 1. Post-natal neovascularization in the physiological or pathological events is consistent with neovessel formation contributed by angiogenesis and vasculogenesis at the various rates between their two mechanisms. Angiogenesis and vasculogenesis are due to the activations of in situ ECs and BM-derived or in situ EPCs, respectively.

endothelial growth factor receptor-2 (VEGFR2), Tie-2, CD117, and stem cell antigen-1 (Sca-1) [13].

The existence of HSCs in the PB and BM, and the demonstration of sustained hematopoietic reconstitution with HSC transplantation led to the idea that a closely related cell-type, namely EPCs, may also exist in adult tissues. Recently, EPCs were successfully isolated from circulating mononuclear cells (MNCs) using VEGFR2, CD34, and CD133 antigens shared by both embryonic EPCs and HSCs [1,14,15]. In vitro, these cells differentiate into endothelial lineage cells, and in animal models of ischemia, heterologous, homologous, and autologous EPCs have been shown to incorporate into the foci of neovasculature, contributing to neovascularization. Recently, similar studies with EPCs isolated from human cord blood have demonstrated their analogous differentiation into ECs in vitro and in vivo [16–19].

These findings have raised important questions regarding fundamental concepts of blood vessel growth and development in adults. Does the differentiation of EPCs in situ (vasculogenesis) play an important role in adult neovascularization, and would impairments in this process lead to clinical diseases? There is now a strong body of evidence suggesting that vasculogenesis in fact significantly contributes to postnatal neovascularization. Recent studies with animal BM transplantation (BMT) models in which BM (donor)-derived EPCs could be distinguished have shown that the contribution of EPCs to neovessel formation may range from 5 to 25% in response to granulation tissue formation [20] or growth factor-induced neovascularization [21]. Also, in the tumor neovascularization, the range is approximately 35–45% higher than the former events [22]. The degree of EPC contribution to post-natal neovascularization is predicted to depend on each neovascularizing event or disease.

3.2. Isolation of EPCs in circulation

Under the current status, it is impossible to differentiate 'immature EPCs' from primitive HSCs, as those cells share common surface markers, i.e. AC133, CD34, or VEGFR2 as described above. In circulation, the cell population with the capacity of differentiation to EPCs is considered to be included in the cell population expressing AC133 and VEGFR2 markers in the subset of CD34 positive cells [15]. Circulating EPCs are constitutively expressing stem/progenitor markers, i.e. CD34 or VEGFR2 except AC133, and start expressing endothelial lineage specific markers, VE cadherin or E-selectin. On the other hand, following the commitment and differentiation to hematopoietic stem/progenitor cells, the surface markers of AC133 and VEGFR2 are extinguished. Such stem/progenitor cell markers do not express on the differentiated hematopoietic cells. Alternatively, kinds of surface markers are expressed to characterize individual hematopoietic cell populations. AC133 is a marker to differentiate immature EPCs or primitive HSCs from circulating EPCs. To differentiate EPCs from hematopoietic stem/progenitor cells, VEGFR2, VE cadherin, or E-selectin are useful. Also, circulating EPCs do not express monocyte or myeloid markers, such as CD14 or CD15. Accordingly, circulating EPCs may be isolated via selection by the antigenicity of CD34, VEGFR2, and/or VE cadherin and also circulating immature EPCs by AC133 (Fig. 2).

3.3. Diverse identification of human EPCs and their precursors

Since the initial report of EPCs [1,2], a number of groups have set out to define this cell population better. Because EPCs and HSCs share many surface markers, and no simple definition of EPCs exists, various methods of EPC isolation have been reported [1,2,15–18,23–31]. The term EPC may therefore encompass a group of cells that exist in a variety of stages ranging from hemangioblasts to fully differentiated ECs. Although the true differentiation lineage of EPCs and their putative precursors remains to be determined, there is overwhelming evidence in vivo that a population of EPCs exists in human.

Lin et al. cultivated peripheral MNCs from patients receiving gender-mismatched BMT and studied their growth in vitro. In this study, they identified a population of BM (donor)-derived ECs with high proliferative potential (late outgrowth); these BM cells likely represent EPCs [24]. Gunsilius et al. investigated a chronic myelogenous leukemia model and disclosed that BM-derived EPCs contribute to postnatal neovascularization in human [26]. Interestingly, in the report, BM-derived EPCs could be detected even in the wall of quiescent vessels without neovascularization events. This finding suggests that BM-derived EPCs may relate even to the turnover of ECs consisting of quiescent vessels.

Reyes et al. have recently isolated multipotent adult progenitor cells (MAPCs) from BM MNCs, differentiated them into EPCs and proposed MAPCs as an origin of EPCs [22]. These studies therefore provide evidence to support the presence of BM-derived EPCs that take part in neovascularization. Also, as described above, the existence of 'in situ EPCs' as derived from tissue specific stem/progenitor cells in murine skeletal muscle remains to be investigated also in the other tissues [5] (Fig. 2).

4. EPC kinetics in adults

4.1. EPC kinetics effected by endogenous agents

The incorporation of BM-derived EPCs into foci of physiological and pathological neovascularization has been demonstrated through various animal experiments. One well-established model that allows the detection of BM-

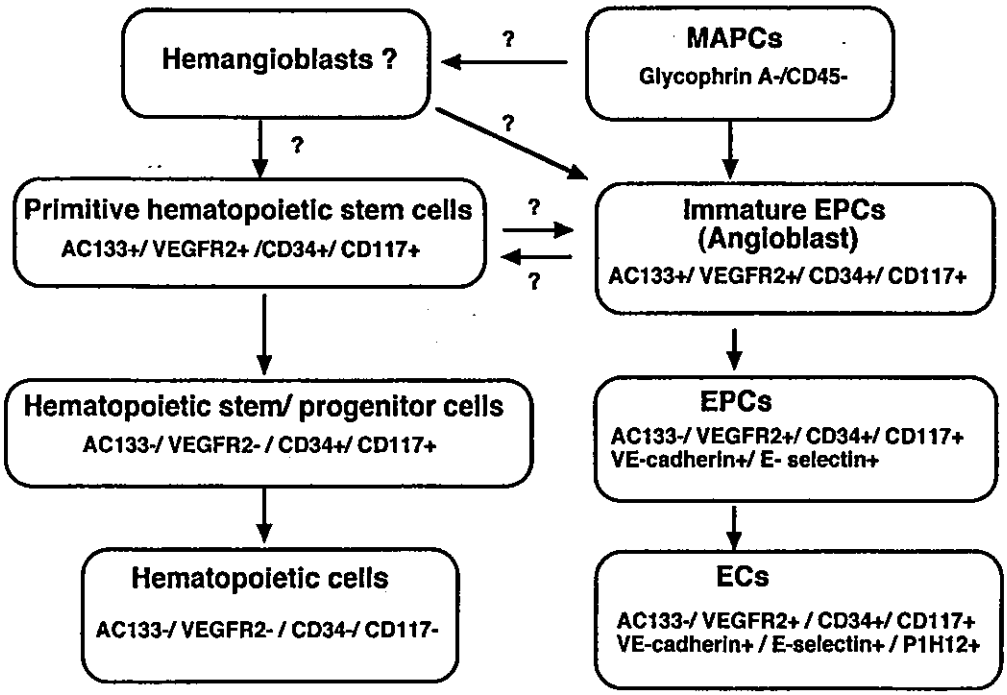

Fig. 2. Origin and differentiation of EPCs in adult BM. EPCs are thought to differentiate not only from putative hemangioblasts, common precursor cells with HSCs, as previously described, but also from MAPCs. Representative antigenicities to stem/progenitor cells are shown (+, positive; −, negative).

derived EPCs includes transplanting wild-type mice with BM cells harvested from transgenic mice in which LacZ expression is regulated by an EC lineage-specific promoter, flk-1 or Tie-2 (flk-1/lacZ/BMT, Tie-2/lacZ/BMT). Using such mice, flk-1- or Tie-2-expressing endothelial lineage cells derived from BM (EPCs) have been shown to localize to vessels during tumor growth, wound healing, skeletal and cardiac ischemia, corneal neovascularization, and endometrial remodeling following hormone-induced ovulation [4].

Tissue trauma causes mobilization of hematopoietic cells as well as pluripotent stem or progenitor cells from the hematopoietic system [32]. Consistent with the notion that EPCs and HSCs share a common ancestry, recent data from our laboratory have shown that mobilization of BM-derived EPCs constitutes a natural response to tissue ischemia. The aforementioned murine BMT model also provided direct evidence of enhanced BM-derived EPC incorporation into foci of corneal neovascularization following the development of hindlimb ischemia [33]. This finding indicates that circulating EPCs are mobilized endogenously in response to tissue ischemia and can incorporate into neovascular foci to promote tissue repair. These results in animals were recently confirmed by human studies illustrating EPC mobilization in patients following burns [6], CABG, or acute myocardial infarction [7].

As previous studies demonstrated, endogenous mobilization of BM-derived EPCs, we considered exogenous mobilization of EPCs as an effective means of augmenting the resident population of EPCs/ECs. Such a strategy is appealing for its potential to overcome the endothelial dysfunction or depletion that may be associated with older, diabetic, or hypercholesterolemic patients. Granulocyte macrophage colony-stimulating factor (GM-CSF) is well known to stimulate hematopoietic progenitor cells and myeloid lineage cells, but has recently been shown to exert a potent stimulatory effect on EPC kinetics. The delivery of this cytokine induced EPC mobilization and enhanced neovascularization of severely ischemic tissues and de novo corneal vascularization [33].

The exact mechanism by which EPCs are mobilized to the peripheral circulation remains unknown, but may mimic aspects of embryonic development. Vascular endothelial growth factor (VEGF), critical for angio/vasculogenesis in the embryo [34–36], has recently been shown to be an important stimulus of adult EPC kinetics. Our studies carried out first in mice [37] and subsequently in patients undergoing VEGF gene transfer for critical limb or myocardial ischemia [38] established that a previously unappreciated mechanism by which VEGF contributes to neovascularization is in part by mobilizing BM-derived EPCs. Similar modulation of EPC kinetics has been observed in response to other hematopoietic stimulators, such as granulocyte-colony stimulating factor (G-CSF) and stroma-derived factor-1 (SDF-1) [39].

4.2. EPC kinetics effected by exogenous agents

EPC mobilization has recently been implicated not only by natural hematopoietic or angiogenic stimulants but also by pharmacological agents. For instance, 3-hydroxy-3-methylglutaryl coenzyme A (HMG-CoA) reductase inhibitors (statins) are known to rapidly activate Akt signaling in ECs, thereby stimulating EC bioactivity in vitro and enhancing angiogenesis in vivo [40]. Recent studies by Dimmeler et al. and our laboratory have demonstrated a novel function of statins by mobilizing BM-derived EPCs through the stimulation of the Akt signaling pathway [41–44]. Therefore this newly appreciated role of statins, along with their already well-established safety and efficacy on hypercholesterolemia, suggests that they can offer benefit in treating various forms of vascular diseases. On the other hand, some antiangiogenic agents, i.e. angiostatin or soluble flk-1, have been shown to inhibit BM-derived EPC kinetics, leading to tumor regression [45], as BM-derived EPC kinetics is a critical factor for tumor growth, in terms of tumor neovascularization [46].

4.3. Clinical profile of EPC kinetics

There is a strong body of evidence to suggest that impaired neovascularization results in part from diminished cytokine production. However, endogenous expression of cytokines is not the only factor leading to impaired neovascularization. Diabetic or hypercholesterolemic animals—like clinical patients—exhibit evidence of dysfunction in mature endothelial cells. While the cellular dysfunction does not necessarily preclude a favorable response to cytokine replacement therapy, the extent of recovery in limb perfusion in these animals fails to reach that of control animals; this suggests another limitation imposed by a diminished responsiveness of EPCs/ECs [47–49].

The aging characterized by impaired neovascularization [50,51] might be associated with dysfunctional EPCs and defective vasculogenesis. Indeed, preliminary results from our laboratory indicate that transplantation of BM (including EPCs) from old mice into young mice led to minimal neovascularization in a corneal micropocket assay, relative to transplantation of young BM. We also demonstrated that EPCs from older patients with clinical ischemia had significantly less therapeutic effect in rescuing ischemic hindlimb of mice compared with those from younger ischemic patients [52]. These studies provide evidence to support an age-dependent impairment in vasculogenesis (as well as angiogenesis) that is heavily influenced by the EPC phenotype. Moreover, analysis of clinical data from older patients at our institution disclosed a significant reduction in the number of EPCs at baseline, as well as that in response to VEGF165 gene transfer [38]. Thus impaired EPC mobilization and/or activity in response to VEGF may contribute to the age-dependent defect in postnatal neovascularization. Recently Vasa et al. have further investigated EPC kinetics and their relationship to clinical disorders, showing that the number and migratory activity of circulating EPCs inversely correlates with risk factors for coronary artery disease, such as smoking, family history and hypertension [53]. On the basis of these findings, monitoring of BM-derived EPC kinetics in the patients with vascular diseases is expected to be valuable in the evaluation of lesion activity and/or therapeutic efficacy.

5. Therapeutic vasculogenesis

5.1. The potential of EPC transplantation

The regenerative potential of stem/progenitor cells is currently under intense investigation. In vitro, stem/progenitor cells possess the capability of self-renewal and differentiation into organ-specific cell types. When placed in vivo, these cells are then provided with the proper milieu that allows them to reconstitute organ systems. The novel strategy of EPC transplantation (cell therapy) may therefore supplement the classic paradigm of angiogenesis developed by Folkman and colleagues. Our studies indicated that cell therapy with culture-expanded EPCs can successfully promote neovascularization of ischemic tissues, even when administered as 'sole therapy,' i.e. in the absence of angiogenic growth factors. Such a 'supply-side' version of therapeutic neovascularization in which the substrate (EPCs/ECs) rather than ligand (growth factor) comprises the therapeutic agent, was first demonstrated by intravenously transplanting human EPCs to immunodeficient mice with hindlimb ischemia [25]. These findings provided novel evidence that exogenously administered EPCs rescue impaired neovascularization in an animal model of critical limb ischemia. Not only did the heterologous cell transplantation improve neovascularization and blood flow recovery, but also led to important biological outcomes—notably, the reduction of limb necrosis and auto-amputation by 50% in comparison with controls. A similar strategy applied to a model of myocardial ischemia in the nude rat demonstrated that transplanted human EPCs localize to areas of myocardial neovascularization, differentiate into mature ECs and enhance neovascularization. These findings were associated with preserved left ventricular (LV) function and diminished myocardial fibrosis [54]. Murohara et al. reported similar findings in which human cord blood-derived EPCs also augmented neovascularization in a hindlimb ischemic model of nude rats, followed by in situ transplantation [17].

More recently, other researchers have explored the therapeutic potential of freshly isolated human CD34+ MNCs (EPC-enriched fraction). Shatteman et al. conducted local injection of freshly isolated human CD34+ MNCs into diabetic nude mice with hindlimb ischemia, and showed an increase in the restoration of limb flow [29].

Similarly Kocher et al. attempted intravenous infusion of freshly isolated human CD34+ MNCs into nude rats with myocardial ischemia, and found preservation of LV function associated with inhibition of cardiomyocyte apoptosis [55]. Thus two approaches of EPC preparation (i.e. both cultured and freshly-isolated human EPCs) may provide therapeutic benefit in vascular diseases, but as described below, will likely require further optimization of techniques to acquire the ideal quality and quantity of EPCs for EPC therapy (Fig. 3).

5.2. Future strategy of EPC cell therapy

Ex vivo expansion of EPCs cultured from PB-MNCs of healthy human volunteers typically yields 5.0×10^6 cells per 100 ml of blood on day 7. Our animal studies [25] suggest that heterologous transplantation requires systemic injection of $0.5–2.0\times10^4$ human EPCs/g body weight of the recipient animal to achieve satisfactory reperfusion of an ischemic hindlimb. Rough extrapolation of these data to human suggests that a blood volume of as much as 12 l may be necessary to obtain adequate numbers of EPCs to treat critical limb ischemia in patients. Therefore, the fundamental scarcity of EPCs in the circulation, combined with their possible functional impairment associated with a variety of phenotypes in clinical patients, such as aging, diabetes, hypercholesterolemia, and homocyst(e)inemia (vide infra), constitute major limitations of primary EPC transplantation. Considering autologous EPC therapy, certain technical improvements that may help to overcome the primary scarcity of a viable and functional EPC population should include: (1) local delivery of EPCs, (2) adjunctive strategies (e.g. growth factor supplements) to promote BM-derived EPC mobilization [33,37], (3) enrichment procedures, i.e. leukapheresis or BM aspiration, or (4) enhancement of EPC function by gene transduction (gene modified EPC therapy, vide infra), (5) culture-expansion of EPCs from self-renewable primitive stem cells in BM or other tissues. Alternatively, unless the quality and quantity of autologous EPCs to satisfy the effectiveness of EPC therapy may be acquired by the technical improvements described above, allogenic EPCs derived from umbilical cord blood or culture-expanded from human embryonic stem cells [17,56], may be available as the sources supplying EPCs.

5.3. Gene modified EPC therapy

A strategy that may alleviate potential EPC dysfunction in ischemic disorders is considered reasonable, given the findings that EPC function and mobilization may be impaired in certain disease states. Genetic modification of EPCs to overexpress angiogenic growth factors, to enhance signaling activity of the angiogenic response, and to

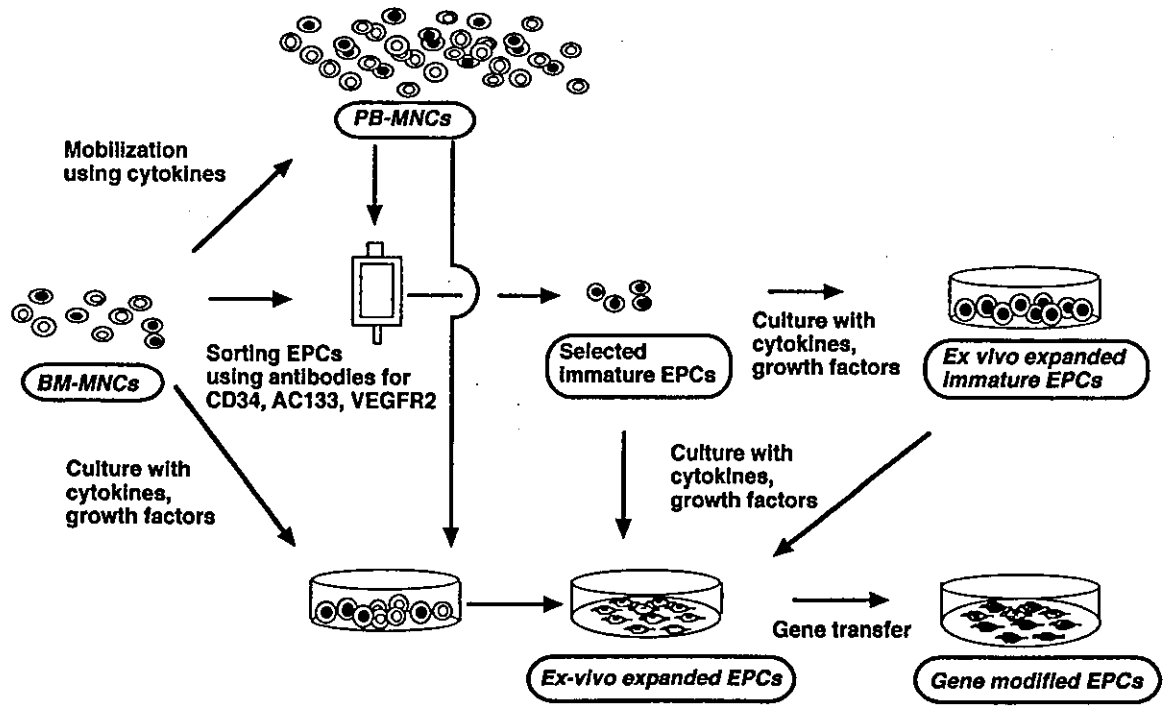

Fig. 3. EPC therapy using autologous EPCs derived from BM for vascular regeneration. Transplantation of BM- or mobilized PB-MNCs are considered 'crude EPC therapy', as EPCs are not selected. BM-MNCs have already been under clinical application. Following the manipulation to acquire the optimized quality and/or quantity, e.g. sorting by surface markers, ex vivo culture-expansion and/or gene transfection, EPC therapy is expected to be the useful strategy for vascular regeneration.